Article

Preparation of Magnetic Dummy Molecularly Imprinted Meso-Porous Silica Nanoparticles Using a Semi-Covalent Imprinting Approach for the Rapid and Selective Removal of Bisphenols from Environmental Water Samples

Jing Chen, Xiaoli Sun *, Muhua Wang, Yan Wang, Qinyao Wu, Shurong Wu and Sisi Fang

Department of Chemistry, Lishui University, Lishui 323000, China
* Correspondence: sxl2015@lsu.edu.cn

Abstract: Bisphenol compounds (BPs) are a severe threat to humans and creatures; hence it is critical to develop a quick and simple approach for removing trace BPs from water. This research synthesized a novel template–monomer complex, phenolphthalein-(3-isocyanatopropyl)triethoxysilane (PP-ICPTES), as a dummy template, and a molecularly imprinted polymer for bisphenol was made via a semi-covalent approach. By successfully coating the imprinted layer on the $Fe_3O_4@SiO_2@mSiO_2$ structure, a magnetic dummy molecularly imprinted mesoporous silica nanoparticles (m-DMI-MSNPs) with a core-shell structure and superefficient aqueous phase selectivity for bisphenols was synthesized. The morphology and structure of the m-DMI-MSNPs were characterized using transmission electron microscopy (TEM), nitrogen adsorption-desorption analysis, Fourier transform infrared spectroscopy (FT-IR), and vibrating sample magnetometry (VSM). The prepared m-DMI-MSNPs presented excellent water compatibility and magnetic separation abilities. The m-DMI-MSNPs showed excellent recognition selectivity towards BPs with imprinting factors of 7.6, 8.2, and 7.5 for bisphenol F (BPF), bisphenol E (BPE), and bisphenol A (BPA), respectively. Fast binding kinetics (equilibrium time < 1 min) and a high rebinding capacity (maximum adsorption capacity, 38.75 mg g^{-1}) were observed in the adsorption experiments. More importantly, the m-DMI-MSNPs, which combine good water compatibility, class selectivity, and magnetic separation performance, exhibited excellent performance for the removal of BPF, BPE, and BPA from tap water, mineral water, and sewage water samples, with removal efficiencies in the ranges of 96.6–97.8, 95.6–97.1, and 93.1–95.3%, respectively.

Keywords: dummy template; semi-covalent imprinting; magnetic nanoparticles; bisphenol; water compatibility

1. Introduction

Bisphenol compounds (BPs) are among the most common environmental endocrine disruptors and represent a serious threat to the human reproductive system, metabolic processes, immune system, and neuroendocrine system [1–3]. Several countries have developed and implemented legislation and guidelines to limit the use of BPA in relevant products and their environmental levels since 2008. The European Chemicals Agency (ECHA) added BPA to its list of high-risk compounds in 2017 [4].

Because relevant legislation places strict restrictions on the use of BPA, BPF, BPE, bisphenol S (BPS), 2,2′-bis(4-hydroxyphenyl)-hexafluoropropane (BPAF), and other BPs are generally utilized as BPA alternatives. However, BPs pollution is prevalent [5]. Liu et al. studied the levels of BPs in surface water in the Pearl River (South China) during the dry season, finding that BPA and BPF were identified at 100% and 84%, respectively [6]. Another study found BPA in 100% of commercially accessible bottled water, while BPA E was found in 24% of samples [7]. As a result, it is critical to conduct an investigation into the removal of BPs.

Molecularly imprinted polymers (MIPs) are three-dimensional porous materials that have been designed with specific target molecules as templates, and their caves can interact with the template molecules in terms of form, size, charge, and functional groups, allowing for effective identification. MIPs have received much attention because of their predictable molecular recognition, high selectivity, excellent chemical stability, ease of synthesis, and structure personalization. MIPs are currently widely used in wastewater treatment, biosensing, separation, and enrichment.

Despite their numerous advantages, the use of MIPs is limited by template molecule leakage. Because template leakage causes secondary contamination, it has a significant impact on trace target removal and detection. A dummy template with a similar structure to the target could be used to solve this problem [8]. This strategy can increase the number of specific binding sites and adsorption capacity while improving analytical method accuracy. Researchers have conducted numerous studies on dummy templates for BPs. Liu et al. [9] compared the extraction effect of MIP prepared with bisphenol B, bisphenol F, 3,3′,5,5′-tetrabromobisphenol (TBBPA), and 4-tert-butylphenol as dummy templates on the actual bisphenol A in water samples. Other researchers have also conducted studies on BPs dummy templates MIPs (DMIPs), such as using 3,3′,5,5′-tetrabromobisphenol (TBBPA) [8], BPAF [10], 4,4′-dihydroxybiphenyl (DDBP) [11], and BPS [12] as dummy templates. These dummy templates have a chemical structure similar to BPA, which eliminates template leakage and improves sensitivity. Unfortunately, the majority of dummy templates have estrogenic effects, which can lead to secondary contamination that is risky to human health and the environment [13]. As a result, developing a highly selective, environmentally friendly, nontoxic, and nonhazardous dummy template for BPs is critical.

In our preliminary work, phenolphthalein (PP) was found to be structurally close to BPA, and the developed PP imprinted polymer had good selectivity towards BPA [14,15]. Using this as a foundation, a brand-new template–monomer complex called PP-ICPTES was synthesized. Magnetic dummy molecularly imprinted mesoporous silica nanoparticles (m-DMI-MSNPs) based on the $Fe_3O_4@SiO_2@mSiO_2$ structure were successfully synthesized employing PP-ICPTES as a dummy template. The contribution of a mesoporous silica shell layer massively improved adsorption capacity, reduced equilibration time, and improved aqueous phase compatibility. The morphology of the synthesized m-DMI-MSNPs, as well as their binding capabilities and adsorption performance on BPs, were thoroughly investigated by applying relevant characterization and adsorption experiments. They have also been employed successfully for the fast and selective removal of BPs from sewage influents.

2. Experimental

2.1. Materials and Apparatus

BPA, BPF, BPE, and catechol (CAT) were purchased from TCI Chemical Reagent Co. Ltd. (Shanghai, China). Tetraethyl orthosilicate (TEOS), cetyltrimethylammonium bromide (CTAB), ammonia water ($NH_3 \cdot H_2O$, 28 wt%), ethanol, hexane, and dimethyl sulfoxide (DMSO) were purchased from Kemiou Chemical Reagent Co. Ltd. (Tianjin, China). 1,1,1-tris(4-hydroxyphenyl)ethane (THPE), 3-aminopropyl triethoxysilane (APTES), (3-isocyanatopropyl)triethoxysilane (ICPTES), ferric chloride hexahydrate ($FeCl_3 \cdot 6H_2O$), anhydrous sodium acetate, ethylene glycol, phenolphthalein (PP), and N, N-dimethylformamide (DMF), dimethyl sulfoxide (DMSO) were purchased from J & K Chemicals (Beijing, China). High-performance liquid chromatography (HPLC) grade acetonitrile and methanol were obtained from Merck (Schwalbach, Germany). Ultrapure water was supplied using a Milli-Q system (Millipore, Bedford, MA, USA).

2.2. Characterisation of the m-DMI-MSNPs and m-NI-MSNPs

Nitrogen adsorption isotherms of the m-DMI-MSNPs and magnetic non-imprinted mesoporous silica nanoparticles (m-NI-MSNPs) were measured using a Nova 4200e analyzer (Quantachrome Instruments, Boynton Beach, FL, USA). Before testing, approximately

60 mg of each sample was degassed for 4 h at 200 °C. The specific surface area (S_{BET}) and porosity were calculated using the Brunauer–Emmett–Teller (BET) and Barret–Joyner–Halenda (BJH) methods, respectively, and parameters, including the specific pore diameter, were then obtained. The morphology of the nanoparticles was observed using a JEM 2100F transmission electron microscope under high vacuum conditions at an accelerating voltage of 200 kV (TEM) (JEOL, Tokio, Japan). An energy dispersive X-ray (EDX) spectrum was obtained on Tecnai G20 (Phillips Electronics Co., Eindhoven, The Netherlands) at an accelerating voltage of 20.0 kV. The structure of the nanoparticles was characterized using Fourier transform infrared (FT-IR) spectroscopy (Nicolet 6700, Thermo Fisher Scientific, Waltham, MA, USA). The template–monomer complex PP-ICPTES was confirmed by proton nuclear magnetic resonance (^{1}H-NMR) (AVANCE NEO 300 MHz, Bruker, Rheinstetten, Germany). The magnetic properties were measured at 25 °C using a vibrating sample magnetometer (VSM 7407, Lakeshore, Carson, CA, USA).

2.3. Preparation of the m-DMI-MSNPs and m-NI-MSNPs

2.3.1. Preparation of Magnetic Fe_3O_4

Spherical Fe_3O_4 nanoparticles were synthesized using a solvothermal method. Typically, 8.1 g $FeCl_3 \cdot 6H_2O$ was dissolved in 300 mL ethylene glycol under magnetic stirring at 500 rpm until a clear yellow solution was obtained. Subsequently, 21.6 g of sodium acetate was added to this solution. After forming a homogeneous dispersion, the mixture was transferred into a Teflon-lined stainless steel autoclave and heated at 200 °C for 8 h. Black magnetic nanoparticles were then separated from the reaction solution using a magnet. The product was washed three times, each with ethanol and deionized water, and dried under vacuum at 60 °C for 24 h.

2.3.2. Preparation of $Fe_3O_4@SiO_2$

$Fe_3O_4@SiO_2$ was prepared according to a previously reported method with some modifications [16]. The steps were as follows the Fe_3O_4 particles (0.1 g) were dispersed in a mixture of isopropyl alcohol (240 mL), deionized water (18 mL), and concentrated aqueous ammonia solution (28 wt%, 21 mL) by ultrasonic vibration. Subsequently, 2 mL TEOS was added dropwise. After stirring for 14 h, the products were collected, washed three times with deionized water, and dried under a vacuum at 60 °C for further use.

2.3.3. Preparation of the Template–Monomer Complexes

The template–monomer complexes PP-ICPTES and THPE-ICPTES were first synthesized. Briefly, dummy template PP or THPE (10 mmol) was dissolved in ultradry DMF solvent (15 mL), and 20 mmol (for PP) or 30 mmol (for THPE) of ICPTES was then added gradually. The mixture was stirred at 80 °C for 48 h under a nitrogen atmosphere. After the reaction was complete, DMF was removed by vacuum distillation. The obtained transparent viscous product was stored under a dry nitrogen atmosphere and characterized using ^{1}H-NMR (300 MHz, $CDCl_3$) analysis.

2.3.4. Preparation of m-DMI-MSNPs and m-NI-MSNPs

Uniform mesoporous $Fe_3O_4@SiO_2@mSiO_2$ were constructed using the typical sol-gel method [16]. Approximately 0.1 g $Fe_3O_4@SiO_2$, prepared in the former step (2.3.2 Preparation of $Fe_3O_4@SiO_2$), was redispersed in a mixed solution containing CTAB (0.30 g, 0.823 mmol), ultrapure water (80 mL), ammonia water (1.0 mL, 28 wt%), and ethanol (60 mL). The mixed solution was homogenized for 0.5 h to form a uniform dispersion. TEOS (0.42 g, 2.0 mmol) and PP-ICPTES (0.15 g, 0.2 mmol) were added to the dispersion under continuous stirring (500 rpm). After reaction for 24 h, the product was collected with a magnet and washed sequentially with ethanol and water three times to remove any nonmagnetic by-products. The PP dummy template was removed by refluxing in DMSO and ultrapure water (5:1, *v/v*) at 180 °C for 3 h. Next, the m-DMI-MSNPs were washed with ethanol by Soxhlet extraction for 12 h to remove the residual DMSO and CTAB

and subsequently dried under vacuum at 60 °C. The corresponding m-NI-MSNPs were prepared using the same procedure, except that APTES was used instead of the template–monomer complex. The schematic procedure for the preparation of the m-DMI-MSNPs is shown in Figure 1.
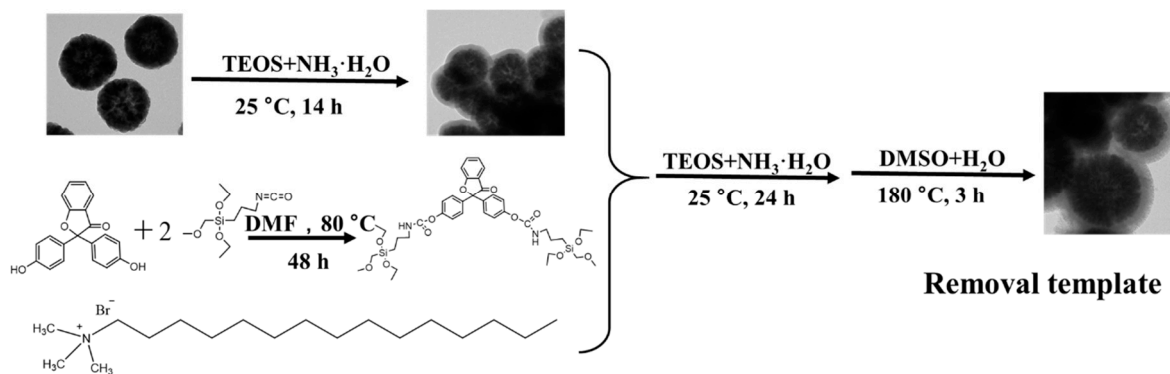
Figure 1. Schematic procedure of preparation of m-DMI-MSNPs.

2.4. Adsorption Experiments of the m-DMI-MSNPs and m-NI-MSNPs

2.4.1. Static Adsorption

The binding capacity (Q) of the M-DMI-MSNPs and m-NI-MSNPs for BPA was determined as follows: exactly 10 mg m-DMI-MSNPs or m-NI-MSNPs was suspended in 2 mL BPA water/methanol (95:5, v/v) solutions with various concentrations ranging from 0.05 to 4.0 mmol L^{-1}. The series of mixtures were shaken for 3 h at 25 °C. After the separation of the magnetic field provided by NdFeB, the residual amount of BPA in the aqueous phase was measured using HPLC. The amount of BPA absorbed by the M-DMI-MSNPs and m-NI-MSNPs was calculated using the following equation:

$$Q_e = \frac{(C_0 - C_t)v}{m} \tag{1}$$

The removal efficiency was calculated using the following equation:

$$\eta = \frac{C_0 - C_t}{C_0} \tag{2}$$

where Q_e (mg g^{-1}) is the mass of BPA adsorbed per unit mass of dry particles, η (%) is the removal efficiency of BPA, C_0 is the initial BPA concentration in solution (mmol L^{-1}), C_t is the residual concentration in the solution at time t (mg L^{-1}), v is the solution volume (mL), and m is the adsorbent mass (g).

Scatchard analysis was used to investigate the binding properties of the obtained m-DMI-MSNPs. The Scatchard plot was constructed according to the following equation [17]:

$$\frac{Q_e}{C_e} = \frac{Q_{max} - Q_e}{K_d} \tag{3}$$

where Q_e is the equilibrium adsorption capacity of the m-DMI-MSNP or m-NI-MSNP material, C_e is the free BPA concentration at equilibrium, K_d is the dissociation constant, and Q_{max} can be obtained from the slope and intercept of the linear line plotted as Q_e/C_e vs. Q_e.

2.4.2. Competition Studies

The class selectivity of the M-DMI-MSNPs was systematically evaluated through procedures similar to those of the static adsorption experiment, using mixture standards of BPA, BPF, BPE, and CAT in ultrapure water/methanol (95:5, v/v). The M-DMI-MSNPs or

m-NI-MSNPs (10 mg) were first dispersed in the mixed standard solution (0.01 mmol L^{-1} of each analyte, 2 mL) and then shaken at 25 °C for 3 h to achieve balanced adsorption. The selectivity of the M-DMI-MSNPs was estimated from the imprinting factor α of the selected BPs between the M-DMI-MSNPs and m-NI-MSNPs. The value of α was determined according to the formula:

$$\alpha = \frac{Q_{\text{MIPs}}}{Q_{\text{NIPs}}} \tag{4}$$

where Q_{MIPs} and Q_{NIPs} are the adsorption capacities for the same analyte of the M-DMI-MSNPs and m-NI-MSNPs, respectively.

2.4.3. Adsorption Equilibrium Time

Kinetic adsorption tests were performed using procedures similar to those used for the static adsorption experiment. Thus, 10 mg M-DMI-MSNPs was suspended in 2 mL of 0.025 mmol L^{-1} BPA ultrapure water/methanol (95:5, v/v) solution. The samples were incubated at 25 °C with shaking. The residual concentrations of the analytes at certain time intervals (1, 2, 3, 4, 5, 7.5, 10, 20, 30, 40, 50, and 60 min) were monitored by HPLC.

2.5. Removal of BPs from the Aqueous Solution

The effect of the sample matrix on the removal efficiency of BPs in tap water, mineral water, and sewage water was next investigated. Mineral water was purchased from the local market in Lishui. Sewage water was obtained from the Lishui Sewage Treatment Plant (Zhejiang province, China, 2021). Specifically, the sewage water samples were collected in glass bottles and filtered through a 0.45 μm filter before freezing for later use. Exactly 10 mg M-DMI-MSNPs were accurately weighed into a 25 mL volumetric bottle with a stopper, after which 10 mL of the water samples spiked at the level of 0.25 mg L^{-1} were added. After ultrasonic treatment for 5 min, the supernatant and nanoparticles were separated using an external magnetic field provided by NdFeB. The amount of residue solution was measured by HPLC.

2.6. HPLC Detection

Quantitative analysis was performed on an Agilent 1260 HPLC system equipped with a diode array detector system and a ZORBAX SB–C18 column (250 mm × 4.6 mm, 5 μm). The mobile phase consisted of ultrapure water and methanol with linear gradient elution, 0–25 min for 35–100% methanol, at a flow rate of 1 mL min^{-1} at 25 °C. The spectra were recorded at 225 nm, and the injection volume was 20 μL.

3. Results and Discussion

3.1. Selection of the Dummy Template

Two new template–monomer complexes PP-ICPTES and THPE-ICPTES, were synthesized for the first time in this research, and their ^{1}H-NMR spectra and chemical reaction equations are given in ESI, Figures S1 and S2. It was found that the addition of different monomer–template complexes altered the creation of ordered mesoporous silica layers in the Fe_3O_4@SiO_2@$mSiO_2$ structure, resulting in a significant variance in the specific surface area of the samples, making it impossible to compare the imprinting effects. The technique of creating sponge mesoporous silica (SMS) materials, in contrast, has the benefits of a straightforward process and a high level of morphological resistance to interference. To compare the imprinting effects of various species of dummy templates, three MIPs were prepared in this study using this technique. This effectively avoided the impact of morphological differences on the imprinting effect, and the specific surface area and pore size results are detailed in ESI Table S1. The specific preparation method of molecularly imprinted sponge mesoporous silica (MISMS) and non-imprinted sponge mesoporous silica NISMS) is detailed in ESI Part 1. Notably, the corresponding non-imprinted material of BPA-MISMS and PP-MISMS is the same, namely NISMS1, but the corresponding non-imprinted material of HPE-MISMS is NISMS2.

By using competitive adsorption, the adsorption efficiency of SMS on BPs was investigated. The findings are displayed in Figure 2A. The imprinting effect has a considerable impact on the removal of BPs by MISMS when compared with NISMS. In particular, the removal of the three BPs demonstrated a considerable improvement for PP-MISMS. Further research into the adsorption patterns of the three MISMs for varying concentrations of BPA in an aqueous solution (0.05–4.0 mM) is presented in Figure 2B. The adsorption capacity of PP-MISM was, as can be seen from the figure, significantly greater than that of the other two, being roughly 3 times that of THPE-MISM. This indicates that in the semi-covalent imprinting system, the MIPs prepared by using PP as a dummy template in the semi-covalent imprinting system were superior to those prepared by THPE. This was different from the consequences of the MIPs prepared using the non-covalent imprinting strategy [14].
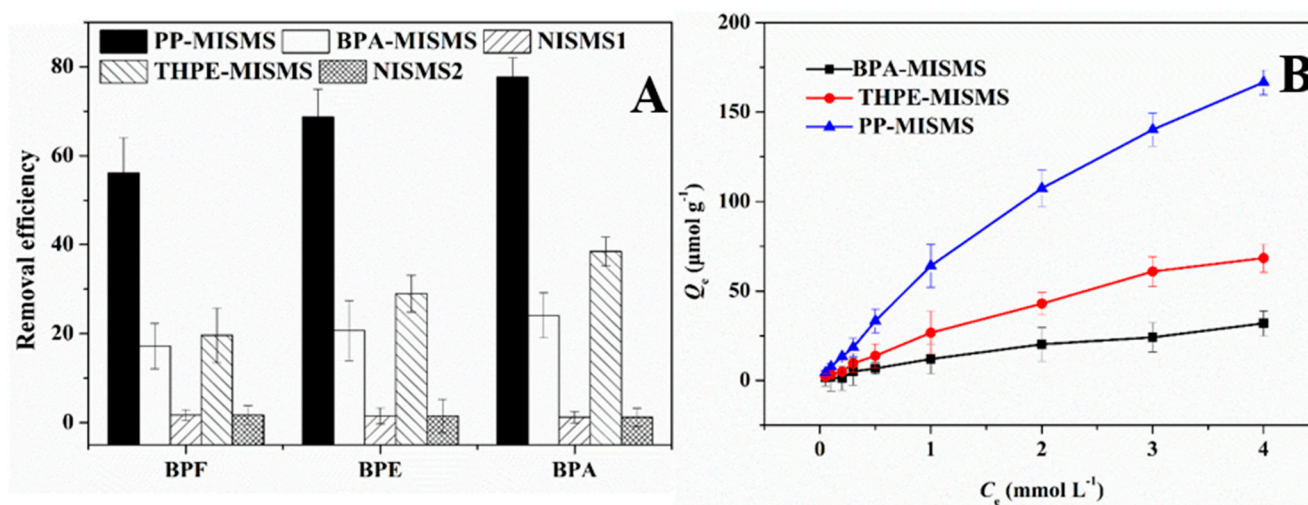

Figure 2. (**A**) The removal efficiency of MISMS prepared by different template molecules on BPs. (**B**) Adsorption isotherms of BPA on PP-MISMS, THPE-MISMS, and BPA-MISMS. The bars represent the mean value $\pm$ standard deviation (*n* = 3).

This might be due to the formation of template–monomer complexes. When the structures of THPE and PP are compared, it is discovered that THPE has three symmetric hydroxyphenyl structures, whereas PP only has two. Because the probability of the three benzene hydroxyl groups interacting with the monomer at the same time is low in the non-covalent imprinting method, and the binding sites are easily accessible during the recognition process, MIPs generated by THPE have more high-affinity sites and a greater imprinting impact. In the semi-covalent imprinting system, however, all three benzene hydroxyl groups of THPE covalently interact with the monomer, and the site is deeply embedded after polymerization. As a result, the recognition process is hampered, and it is more difficult for BPs to approach the binding site, which reduces selectivity. To summarize, the effect of PP as a dummy template has significant advantages in the semi-covalent blotting system, so we use PP as a dummy template for further follow-up studies.

Morphology and Characterization

The morphologies of the Fe_3O_4 nanoparticles, $Fe_3O_4@SiO_2$ nanoparticles, m-DMI-MSNPs, and m-NI-MSNPs were characterized by TEM, and the resulting patterns are shown in Figure 3. As shown in Figure 3A, the magnetic Fe_3O_4 nanoparticles were spherical with good dispersion and uniform particle size with an average value of approximately 321 nm. As illustrated in Figure 3B, the Fe_3O_4 nanoparticles were fully coated with a silicon shell with a thickness of approximately 30 nm to protect them from being oxidized and facilitate further loading of the mesoporous silicon layer. Moreover, the $Fe_3O_4@SiO_2$ nanoparticles were coated with a meso-silica shell to improve their capacity. As can be seen from Figure 3C,D, based on the first silicon shell, a layer of ordered mesoporous silicon is

further covered, and the pore structure is visible. This was attributed to the addition of the PP-ICPTES template–monomer complexes, resulting in a slight difference in the thickness of the mesoporous load layer between the imprinted and non-imprinted materials. According to the statistical analysis (Figure S3, ESI), the particle sizes of the m-DMI-MSNPs and m-NI-MSNPs were 461.22 ± 80.07 nm and 471.90 ± 64.48 nm, respectively. Furthermore, the EDX spectrum in Figure S4 demonstrates that the m-DMI-MSNPs include 24. 34% C, 10.97% N, 46.01% O, 12.45% Si, and 6.23% Fe. The Fe signal in the figure could be due to a lack of consistent local particle wrapping. The existence of components, such as N and Si, can demonstrate the graft of imprinted polymer onto the surface of $Fe_3O_4@SiO_2$.
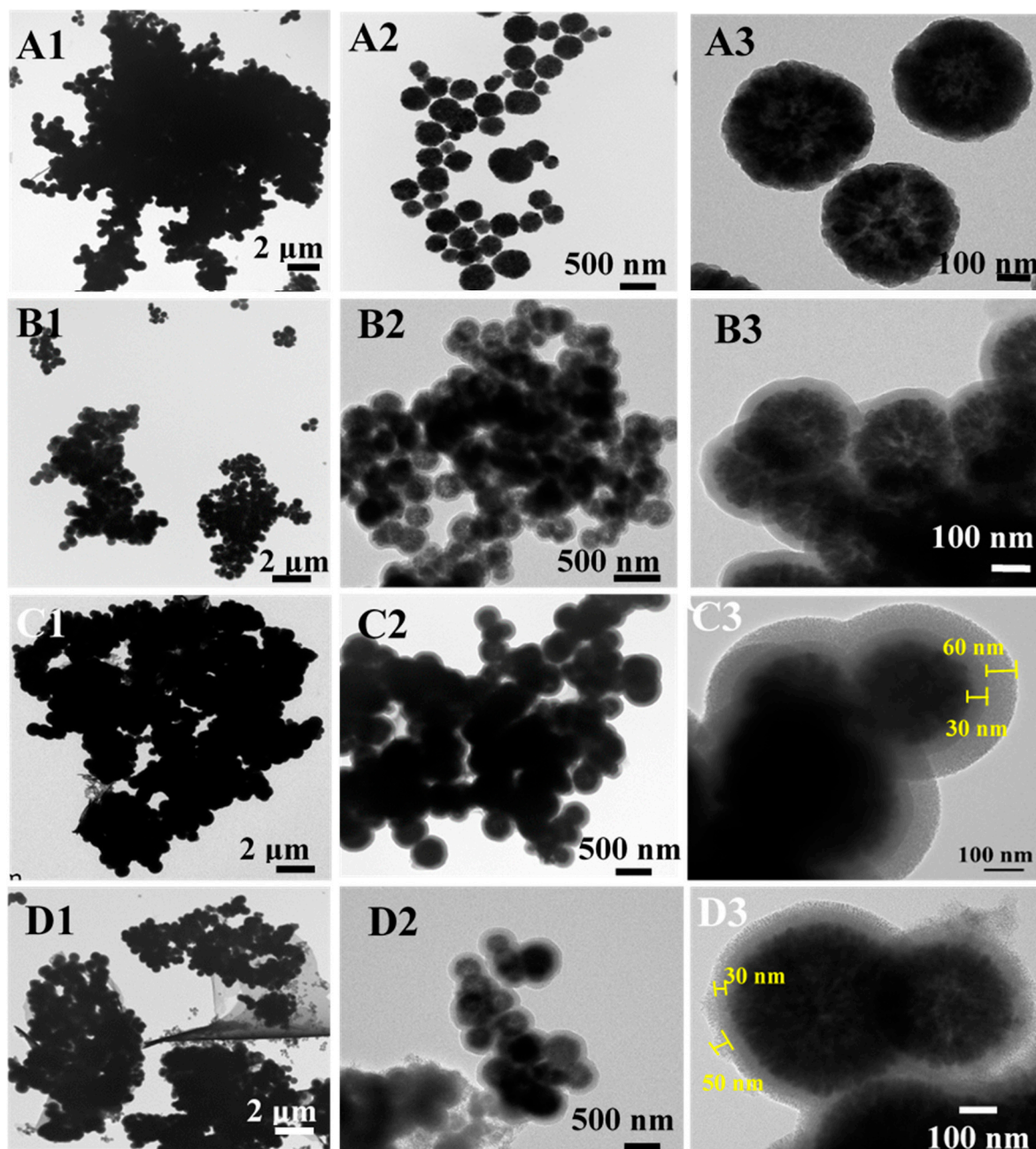
Figure 3. TEM image (**A**) Fe_3O_4; (**B**) $Fe_3O_4@SiO_2$; (**C**) m-NI-MSNPs; (**D**) m-DMI-MSNPs.

Following the BET analysis, the m-DMI-MSNPs and m-NI-MSNPs showed the typical IV isotherm adsorption lag characteristics, as depicted in Figure 4A, suggesting the presence of numerous mesopores in the m-DMI-MSNPs and m-NI-MSNPs. Meanwhile, the rise

in the adsorption ability in the curve at the lower relative pressure ($p/p_0 < 0.2$) indicated the existence of micropores. The specific surface areas of the m-DMI-MSNPs and m-NI-MSNPs were determined as 91.32 and 87.98 $m^2\ g^{-1}$, respectively. Figure 4B exhibits the corresponding pore size distribution plots computed from the adsorption branch of the nitrogen adsorption isotherm using the BJH method. The pore diameters of 3.58 and 2.55 nm for m-DMI-MSNPs and m-NI-MSNPs, respectively, suggest that the addition of the template–monomer complex may have caused some pore structures to collapse during polymerization, resulting in a slight increase in the pore size of m-DMI-MSNPs. However, the difference with m-NI-MSNPs was not significant. Therefore, the difference in the adsorption properties of m-DMI-MSNPs and m-NI-MSNPs is mainly attributed to the imprinting effect rather than morphological differences.
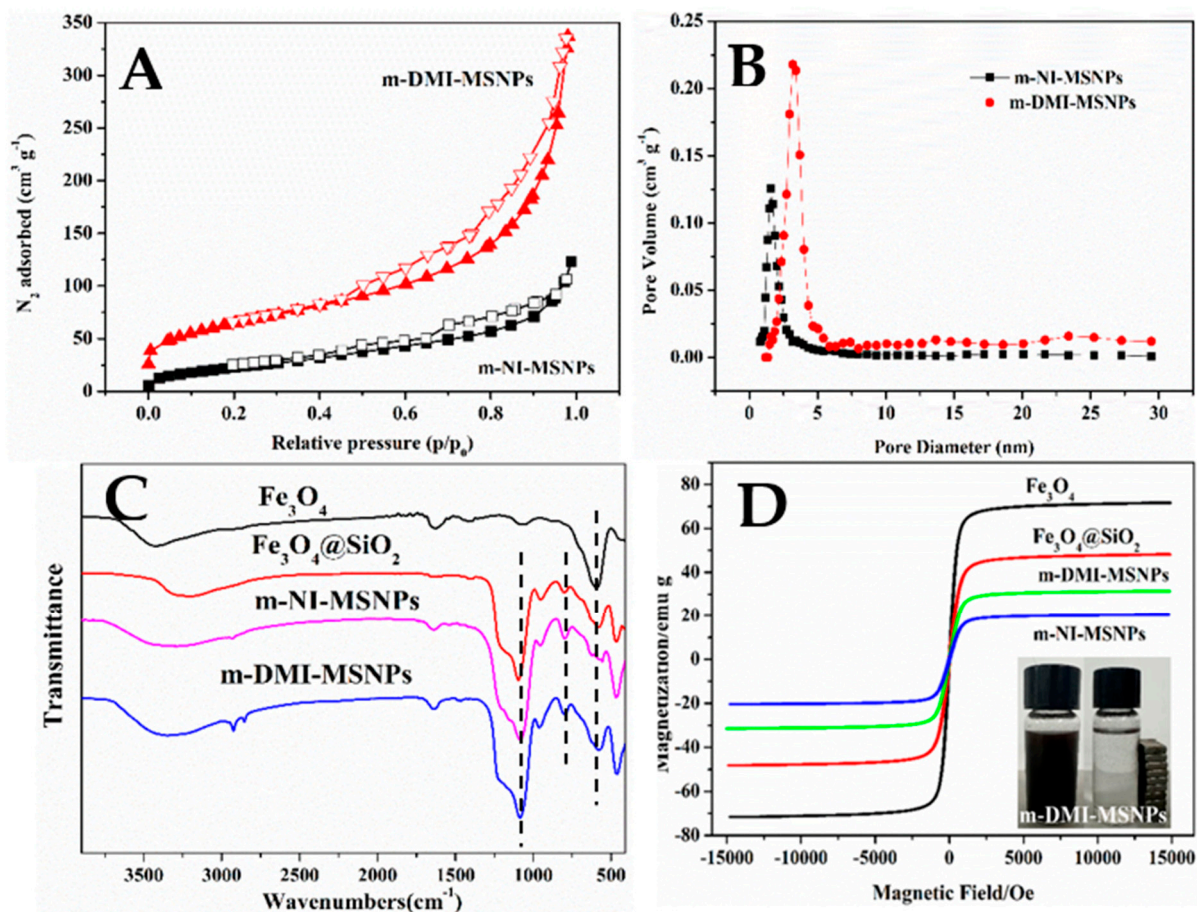
Figure 4. (**A**) N_2 sorption isotherm curve of m-NI-MSNPs and m-DMI-MSNPs, (**B**) BJH pore-size distribution of m-NI-MSNPs and m-DMI-MSNPs, (**C**) FT-IR spectra of Fe_3O_4, $Fe_3O4@SiO_2$, m-DMI-MSNPs, and m-NMI-MSNPs, and (**D**) VSM spectroscopy, inset: photographs of m-DMI-MSNPs suspended in BPA.

The FT-IR spectra of the Fe_3O_4, $Fe_3O_4@SiO_2$, m-DMI-MSNPs, and m-NI-MSNPs are compared in Figure 4C. As illustrated in spectrum a, Fe_3O_4 particles have a typical band at 585 cm^{-1}, which is related to Fe–O stretching [17]. The adsorption bands located at 3446, 1614, and 1406 cm^{-1} can be attributed to the O–H, C=O, and C–O stretching vibrations, respectively, indicating the presence of numerous carboxylic acid groups, which are crucial for the subsequent coating [18]. After the silica coating process, the $Fe_3O_4@SiO_2$ nanoparticles presented new absorption bands at 795 and 1095 cm^{-1}, respectively, corresponding to Si–O–Si symmetric and asymmetric stretching vibrations [19]. These results indicate that the surface of the Fe_3O_4 nanoparticles was successfully coated with silica. A comparison of M-DMI-MSNPs and m-NI-MSNPs reveals that the m-NI-MSNPs have similar functional

groups, shapes, and positions to the m-DMI-MSNPs. The only difference is the C–H peaks at 2924 and 2846 cm^{-1}, which could be due to PP-ICPTES not being eliminated during the elution of the m-DMI-MSNPs.

VSM was used to characterize the magnetic properties of the Fe$_3$O$_4$, Fe$_3$O$_4$@SiO$_2$, m-DMI-MSNP, and m-NI-MSNP samples. The magnetic hysteresis loops of the materials are shown in Figure 4D. The four curves are similar and symmetric near the origin, indicating that the prepared materials are superparamagnetic. Notably, the saturation magnetization of Fe$_3$O$_4$ (70.45 emu g^{-1}) is similar to that reported in the literature and much stronger than those of Fe$_3$O$_4$@SiO$_2$ (46.98 emu g^{-1}), m-DMI-MSNPs (30.68 emu g^{-1}), and m-NI-MSNPs (19.64 emu g^{-1}) [20]. This indicates that the silica shell effectively shields the Fe$_3$O$_4$ core, thereby significantly reducing its magnetic response. Although the saturation magnetization of the m-DMI-MSNPs was reduced compared with that of pure Fe$_3$O$_4$, the m-DMI-MSNPs still showed strong magnetism and could be separated rapidly under an external magnetic field provided by NdFeB.

3.2. Binding Properties

3.2.1. Adsorption Isotherm

A static adsorption test was performed to evaluate the imprinting effect of the m-DMI-MSNP material on BPA. The adsorption isotherms of BPA on the m-DMI-MSNP and m-NI-MSNP materials are shown in Figure 5A. The equilibrium adsorption capacities (Q_e) of the m-NI-MSNP and m-DMI-MSNP materials for BPA both increased with increasing BPA concentration. However, the amounts of BPA adsorbed on the m-DMI-MSNPs were much higher than those adsorbed on the m-NI-MSNPs in the initial concentration range of 0.05–4.0 mmol L^{-1}, indicating that the former material has a more significant imprinting effect towards BPA. As the initial concentration of BPA increased, the equilibrium adsorption capacity (Q_e) for BPA first increased significantly, then slowed down, and finally reached equilibrium, as expected. This trend is mainly attributed to the presence of affinity-binding sites created by the molecular imprinting process. These results showed that the imprinting strategy used in this study was successful. The adsorption isotherms of BPA on m-DMI-MSNPs and m-NI-MSNPs show a typical Langmuir adsorption (Figure S5, ESI), indicating monolayer adsorption with a limited number of sites on the sorbent. The maximum BPA adsorption of MDMIPs was calculated to be 38.75 mg g^{-1}, which was 25.04 mg g^{-1} higher than that of the corresponding MNIPs (13.71 mg g^{-1}).

Figure 5B clearly illustrates that there are two apparent sections within the plot, which can be considered as two straight lines for the m-DMI-MSNPs but only one for m-NI-MSNPs. The results imply that the two different straight lines of the former sorbent correspond to the high- (specific) and low- (nonspecific) affinity binding sites, indicating that the binding sites in the m-DMI-MSNPs were heterogeneous. This type of semi-covalent molecular imprinting polymer is quite common because different compounds are formed by the bonding between the imprinted molecule and functional monomer. The corresponding K_d and Q_{max} values were calculated from the slopes and intercepts of the two linear portions of the Scatchard plot. For the m-DMI-MSNPs, K_d and Q_{max} were respectively calculated as 0.64 mmol L^{-1} and 133.10 μmol g^{-1} for the high-affinity binding sites and 16.17 mmol L^{-1} and 1112.61 μmol g^{-1} for the low-affinity binding sites. For the m-NI-MSNPs, K_d and Q_{max} were 1.47 mmol L^{-1} and 60.75 mol g^{-1}, respectively.
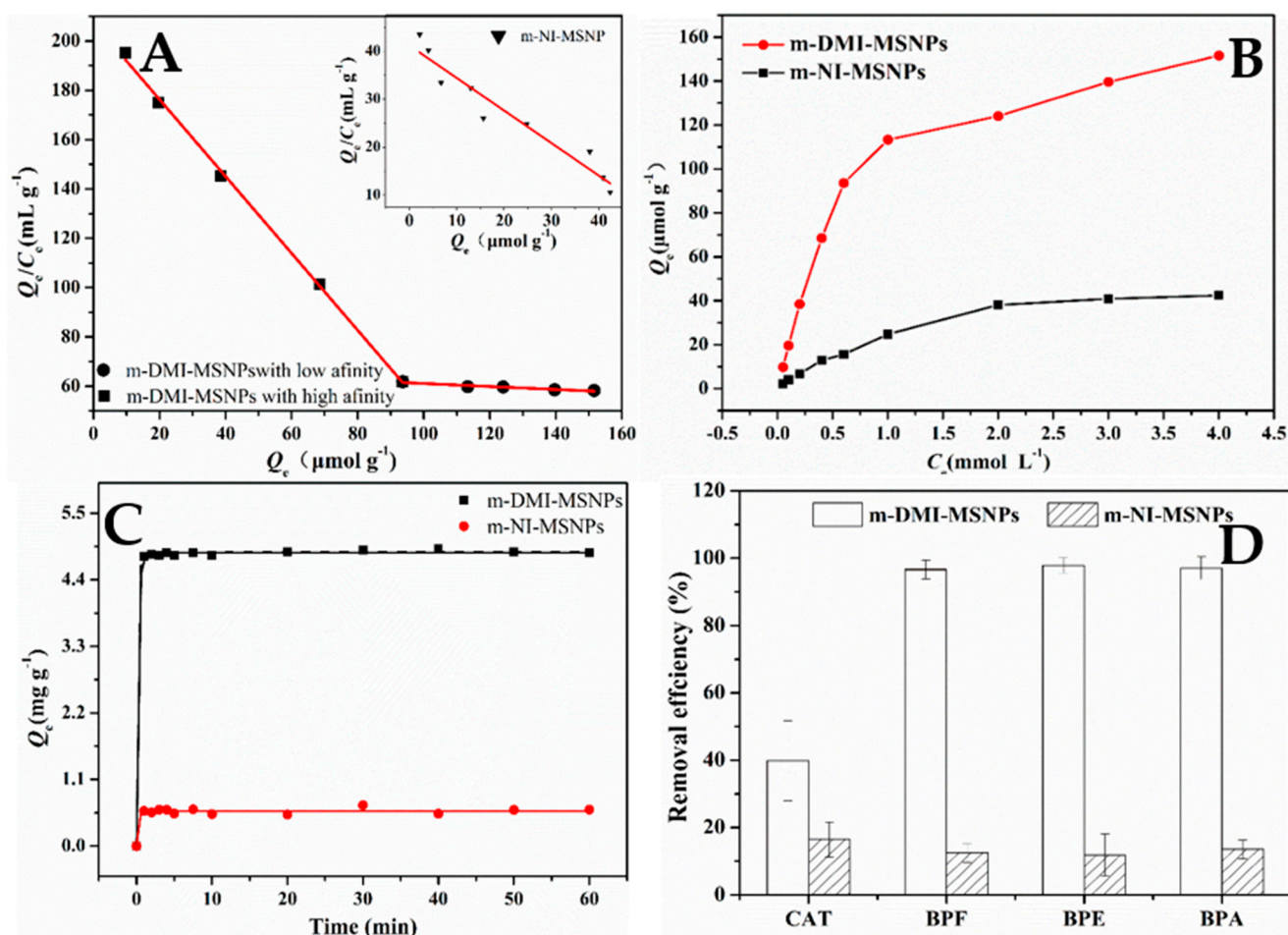
Figure 5. (**A**) Adsorption isotherms of BPA on m-DMI-MSNPs and m-NI-MSNPs, (**B**) Scatchard analysis for m-DMI-MSNPs and m-NI-MSNPs, (**C**) Adsorption kinetics of m-DMI-MSNPs and m-NI–MSNPs, (**D**) Removal efficiency of m–DMI–MSNPs and m-NI–MSNPs towards BPs. The bars represent the mean value ± standard deviation (*n* = 3).

Usually, a lower K_d and higher Q_{max} indicate a higher binding affinity and capacity, respectively. The BPA adsorption capacity of the m-NI-MSNPs was much lower than that of the m-DMI-MSNPs. This suggests that specific adsorption of the m-DMI-MSNPs was achieved by imprinting, while the m-NI-MSNPs did not have specific binding sites matching BPA and, thus, only displayed poor nonspecific adsorption.

3.2.2. Adsorption Equilibrium Time

The adsorption kinetics of BPA on the m-DMI-MSNPs and m-NI-MSNPs were investigated at different time intervals (1–60 min) to study the adsorption rate. As shown in Figure 5C, significant binding equilibria occurred on the two sorbents within 1 min, after which no appreciable changes in terms of binding were observed. However, notably, a much higher BPA binding capacity was observed for the m-DMI-MSNPs than for the m-NI-MSNPs. These results indicate that the molecular imprinting process resulted in the formation of specific recognition sites on the surface of the m-DMI-MSNPs. The nanometer thickness of the imprinted silica film on the surface of the magnetic core was beneficial to the mass transfer of BPA molecules in and out of the imprinted cavities. On considering the convenience of operation and the parallelism of experimental operation, 10 min was chosen as the adsorption time. Moreover, the relationship between removal efficiency and solution pH was investigated (Figure S6, ESI). In general, MMIP demonstrated that BPs were removed most effectively under neutral settings and more effectively under

alkaline conditions than under acidic conditions. This might be because BPs dissociate under alkaline conditions and decrease their ability to bind to the imprinted sites, which affects their adsorption capability. Due to electrostatic repulsion and competition from free hydrogen ions in solution, the adsorption capacity was considerably decreased in acidic conditions [21,22].

3.2.3. Adsorption Selectivity

To further research the class selectivity of m-DMI-MSNPs for BPs, the adsorption of three BPs with high detection rates in water, BPA, BPF, and BPE, as well as CAT the structural analogs of BPs, on m-DMI-MSNP and m-NI-MSNPs was investigated in this paper.

As shown in Figure 5D, the supernatant of the standard mixture was adsorbed by both sorbents. Based on the changes in the relative BPs contents, a difference in the m-DMI-MSNP and m-NI-MSNP sorbent selectivities was suggested. Indeed, the m-DMI-MSNPs exhibited excellent adsorption performance for BPs and revealed a significantly higher BP adsorption amount than that observed with the m-NI-MSNPs. Thus, we concluded that the m-DMI-MSNPs have good selectivity for BPs. The selectivity of the m-DMI-MSNPs can be estimated from the imprinting factor α of the selected BPs between the m-DMI-MSNPs and m-NI-MSNPs. The value of α is equal to or greater than unity, which indicates the excellent imprinting efficiency of the proposed method. The α values towards CAT, BPF, BPE, and BPA were calculated as 2.3, 7.6, 8.2, and 7.5, respectively.

According to the above results, the m-DMI-MSNPs have a much higher selectivity for BPs than for the CAT structural analogs. This was mainly attributed to the formation of specific recognition sites for BP compounds in the process of the molecularly imprinted layer. Although CAT has similar functional (hydroxyl) groups, the cavities cannot match them as tightly as those of the BPs. Compared with the m-NI-MSNPs, m-DMI-MSNPs have excellent selectivity towards BPs. This is largely because m-DMI-MSNPs lack cavities similar in size and structure to BPs, and their functional groups are scattered and dispersed.

The above results are in agreement with the expectation that the selectivity of m-DMI-MSNPs for BPs is much higher than that of CAT. This is mainly due to the formation of specific recognition sites for BPs compounds during the process of molecularly imprinted layers. Although CAT has similar functional groups (hydroxyl groups), their cavities cannot be matched as closely as BPs and thus are less selective. Compared with m-NI-MSNPs, m-DMI-MSNPs have good selectivity for BPs. This is mainly due to the introduction of template molecules, which led to the formation of cavities of similar size and structure to BPs on m-DMI-MSNPs during the cross-linking process, thus substantially improving their selectivity. While m-NI-MSNPs do not have such cavities, their functional groups are more distributed, resulting in a decrease in selectivity.

3.3. Application of m-DMI-MSNPs in Water Samples

The m-DMI-MSNPs were then used as a promising candidate for the efficient adsorption and removal of typical BPs (BPA, BPE, and BPF) from an aqueous solution. Figure 6A displays the results of our investigation into the removal effect of 10 mg m-DMI-MSNPs on BPs at different concentrations (0.25–5.00 mg L^{-1}). The removal efficiency of BPs by m-DMI-MSNPs steadily declined with an increase in BPs concentration. This was mostly because m-DMI-MSNPs gradually approached adsorption saturation. Interestingly, the removal efficiency of BPs by m-DMI-MSNPs was up to more than 95% when the BPs content was at 0.25 mg L^{-1}, indicating that m-DMI-MSNPs have a very high selectivity for trace BPs pollutants in an aqueous solution.
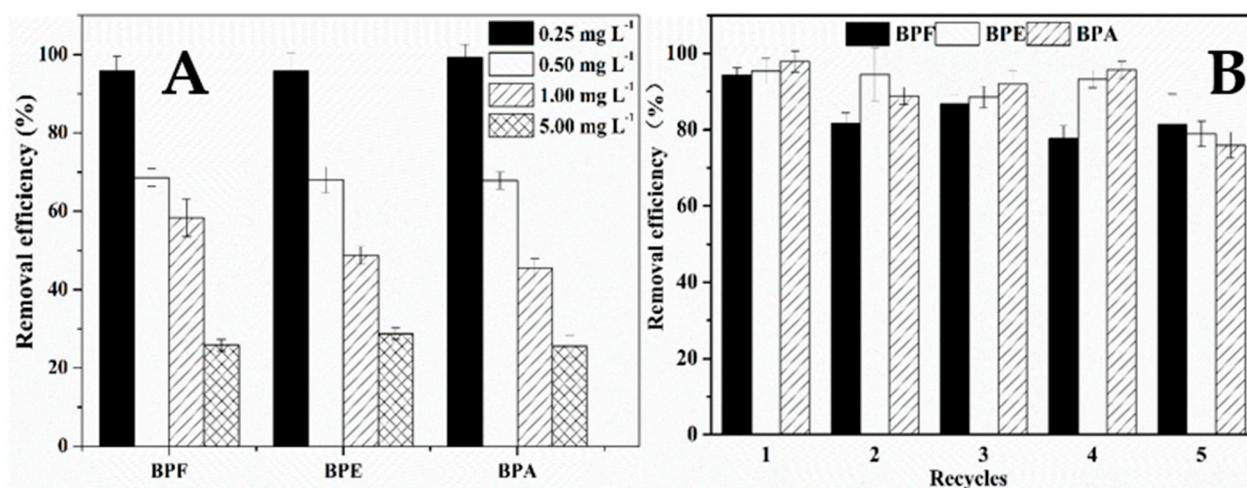
Figure 6. (**A**) Removal efficiency of m-DMI-MSNPs and m-NI-MSNPs towards BPs, and (**B**) the recycle test of the m-DMI-MSNPs. The bars represent the mean value $\pm$ standard deviation (*n* = 3).

Methanol was used as the elution solvent in this study to examine the effects of five consecutive cycles of BPs (0.25 mg L^{-1}) adsorption-desorption by m-DMI-MSNPs. Figure 6B demonstrates that after five cycles, the removal efficiency of m-DMI-MSNP for BPs remained relatively constant at around 80%, demonstrating that they exhibited strong physical stability and regeneration. And the TEM images of particle after adsorption and regeneration of m- DMI-MSNP were shown in Figure S7.

To evaluate the effect of matrix interference, we tested the removal efficiency of BPs by m-DMI-MSNPs in 10 mL of tap water, mineral water, and sewage turn. Sewage was taken from a wastewater treatment plant (Lishui, China), filtered, and placed in a dark place at 4°C for storage until use. Tap water is taken from our laboratory's water pipes. Mineral water was purchased from a local supermarket. The results are shown in Table 1. According to the data in Table 1, m-DMI-MSPNs have good selective adsorption ability on BPF, BPE, and BPA, with removal rates of 96.6–97.8, 95.6–97.1, and 93.1–95.3%, respectively. This demonstrates that m-DMI-MSPNs can remove BPs from real wastewater without any pretreatment, even when the sample volume is scaled up to 10 mL.

Table 1. The removal efficiency of m-DMI-MSNPs towards BPs.

	Tap Water		Mineral Water		Sewage Influents	
	$\eta \pm$ SD (%)	RSD (*n* = 3)	$\eta \pm$ SD (%)	RSD (*n* = 3)	$\eta \pm$ SD (%)	RSD (*n* = 3)
BPF	96.62 $\pm$ 2.71	2.8%	95.55 $\pm$ 1.44	1.5%	93.07 $\pm$ 6.33	6.8%
BPE	97.84 $\pm$ 2.25	2.3%	97.13 $\pm$ 1.36	1.4%	94.29 $\pm$ 1.32	1.4%
BPA	97.08 $\pm$ 3.20	3.3%	96.73 $\pm$ 2.81	2.9%	95.33 $\pm$ 2.19	2.3%

3.4. Comparison of the MMIP Properties for BPs

Table 2 presents a comparison of several magnetic molecular imprinting polymers on BPA molecules. In comparison to previously released studies, the m-DMI-MSPNs compounds prepared in this investigation demonstrated an amazingly imprinting factor (α = 7.5), extremely fast adsorption kinetics (Equilibrium time <1 min), a relatively high adsorption capacity (Q_{max} = 38.75 mg g^{-1}) and good magnetic characteristics (30.68 emu g^{-1}). This is primarily because m-DMI-MSPNs are synthesized using a semi-covalent imprinting technique and are capable of synergistic recognition by non-covalent bonding, hydrogen bonding, and intermolecular interactions during the adsorption process, resulting in super selectivity and huge adsorption capacity. Additionally, m-DMI-MSPNs use PP as a dummy template not only to avoid template leakage but also to be more environmentally friendly than traditional alternative templates such as BPAF and 4,4'-Biphenol.

Table 2. Comparison of different magnetic molecular imprinting adsorbents for BPA.

Template	α	Q_{max} (mg g^{-1})	Saturation Magnetization (emu g^{-1})	Equilibrium Time (min)	Reference
BPA	4.1	21.30	0.14	20	[23]
BPA	1.4	0.39	60	5	[24]
BPA	1.71	60	-	10	[25]
BPA	4.25	8.97	29.01	240	[26]
BPA	11.19	50.92	24.58	5	[27]
BPA	1.10	105.5	<6	60	[22]
BPA	3.87	17.98	35.18	40	[28]
BPA	3.95	8.29	38.3	500	[18]
BPA	3.29	11.00	41.1	15	[29]
BPA	3.5	122.2	28.01	120	[30]
PTOP	1.8	10.64	26.52	20	[31]
BPF	1.3	26.53	30.1	5	[32]
BPAF	-	5.92	37.75	2	[33]
4,4′-Biphenol	4.8	76.80	4.87	180	[8]
DDBP	2.04	101.49	47.60	30	[11]
PP	7.5	38.75	30.68	<1	This work

4. Conclusions

We present a novel dummy template for BPs (PP-ICPTES), a new magnetic molecularly imprinted nanoparticles with a core-shell structure synthesized by a semi-covalent imprinting process combined with surface imprinting and magnetic separation techniques. The m-DMI-MSNP prepared in this study exhibits outstanding chemical stability and magnetic characteristics, as well as great aqueous phase compatibility with BPs. Compared with existing magnetic adsorption materials for BPs, m-DMI-MSNP offers the benefits of excellent selectivity, facile magnetic separation, high adsorption capacity, and fast equilibrium. m-DMI-MSNP has a high potential for rapid adsorption and removal of trace BPs pollutants from aqueous solutions.

Author Contributions: Conceptualization, X.S. and J.C.; methodology, J.C. and Q.W.; validation, S.W. and S.F.; formal analysis, J.C. and M.W.; investigation, J.C.; writing—original draft preparation, J.C., Y.W. and M.W.; writing—review and editing, J.C. and X.S.; funding acquisition, X.S. All authors have read and agreed to the published version of the manuscript.

Institutional Review Board Statement: Not applicable.

Informed Consent Statement: Not applicable.

Conflicts of Interest: The authors declare no conflict of interest.

References

1. Lin, Z.; Cheng, W.; Li, Y.; Liu, Z.; Chen, X.; Huang, C. A Novel Superparamagnetic Surface Molecularly Imprinted Nanoparticle Adopting Dummy Template: An Efficient Solid-Phase Extraction Adsorbent for Bisphenol A. *Anal. Chim. Acta* **2012**, *720*, 71–76. [CrossRef] [PubMed]
2. Huang, C.; Wu, L.-H.; Liu, G.-Q.; Shi, L.; Guo, Y. Occurrence and Ecological Risk Assessment of Eight Endocrine-Disrupting Chemicals in Urban River Water and Sediments of South China. *Arch. Environ. Contam. Toxicol.* **2018**, *75*, 224–235. [CrossRef] [PubMed]
3. Zhao, W.; Bi, X.; Peng, Y.; Bai, M. Research Advances of the Phosphorus-Accumulating Organisms of Candidatus Accumulibacter, Dechloromonas and Tetrasphaera: Metabolic Mechanisms, Applications and Influencing Factors. *Chemosphere* **2022**, *307*, 135675. [CrossRef] [PubMed]
4. Wan, M.L.Y.; Co, V.A.; El-Nezami, H. Endocrine Disrupting Chemicals and Breast Cancer: A Systematic Review of Epidemiological Studies. *Crit. Rev. Food Sci. Nutr.* **2022**, *62*, 6549–6576. [CrossRef]
5. den Braver-Sewradj, S.P.; van Spronsen, R.; Hessel, E.V.S. Substitution of Bisphenol A: A Review of the Carcinogenicity, Reproductive Toxicity, and Endocrine Disruption Potential of Alternative Substances. *Crit. Rev. Toxicol.* **2020**, *50*, 128–147. [CrossRef]
6. Wang, H.; Tang, Z.; Liu, Z.; Zeng, F.; Zhang, J.; Dang, Z. Occurrence, Spatial Distribution, and Main Source Identification of Ten Bisphenol Analogues in the Dry Season of the Pearl River, South China. *Environ. Sci. Pollut. Res.* **2022**, *29*, 27352–27365. [CrossRef]
7. Wang, H.; Liu, Z.; Tang, Z.; Zhang, J.; Yin, H.; Dang, Z.; Wu, P.; Liu, Y. Bisphenol Analogues in Chinese Bottled Water: Quantification and Potential Risk Analysis. *Sci. Total Environ.* **2020**, *713*, 136583. [CrossRef]
8. Wang, Y.; Tian, M.; Yu, K.; Li, L.; Zhang, Z.; Li, L. A Versatile Strategy to Fabricate Magnetic Dummy Molecularly Imprinted Mesoporous Silica Particles for Specific Magnetic Separation of Bisphenol A. *New J. Chem.* **2019**, *43*, 3400–3408. [CrossRef]
9. Liu, Y.; Wang, D.; Du, F.; Zheng, W.; Liu, Z.; Xu, Z.; Hu, X.; Liu, H. Dummy-Template Molecularly Imprinted Micro-Solid-Phase Extraction Coupled with High-Performance Liquid Chromatography for Bisphenol A Determination in Environmental Water Samples. *Microchem. J.* **2019**, *145*, 337–344. [CrossRef]
10. Zhang, J.; Chen, Y.; Wu, W.; Wang, Z.; Chu, Y.; Chen, X. Hollow Porous Dummy Molecularly Imprinted Polymer as a Sorbent of Solid-Phase Extraction Combined with Accelerated Solvent Extraction for Determination of Eight Bisphenols in Plastic Products. *Microchem. J.* **2019**, *145*, 1176–1184. [CrossRef]
11. Chang, T.; Yan, X.; Liu, S.; Liu, Y. Magnetic Dummy Template Silica Sol–Gel Molecularly Imprinted Polymer Nanospheres as Magnetic Solid-Phase Extraction Material for the Selective and Sensitive Determination of Bisphenol A in Plastic Bottled Beverages. *Food Anal. Methods* **2017**, *10*, 3980–3990. [CrossRef]
12. Kubiak, A.; Ciric, A.; Biesaga, M. Dummy Molecularly Imprinted Polymer (DMIP) as a Sorbent for Bisphenol S and Bisphenol F Extraction from Food Samples. *Microchem. J.* **2020**, *156*, 104836. [CrossRef]
13. Lee, J.; Moon, K.W.; Ji, K. Systematic Review of Exposure to Bisphenol A Alternatives and Its Effects on Reproduction and Thyroid Endocrine System in Zebrafish. *Appl. Sci.* **2021**, *11*, 1837. [CrossRef]
14. Sun, X.; Wang, J.; Li, Y.; Jin, J.; Yang, J.; Li, F.; Shah, S.M.; Chen, J. Highly Class-Selective Solid-Phase Extraction of Bisphenols in Milk, Sediment and Human Urine Samples Using Well-Designed Dummy Molecularly Imprinted Polymers. *J. Chromatogr. A* **2014**, *1360*, 9–16. [CrossRef]
15. Yang, J.; Li, Y.; Huang, C.; Jiao, Y.; Chen, J. A Phenolphthalein-Dummy Template Molecularly Imprinted Polymer for Highly Selective Extraction and Clean-Up of Bisphenol A in Complex Biological, Environmental and Food Samples. *Polymers* **2018**, *10*, 1150. [CrossRef]
16. Xiong, X.; Li, D.; Du, Z.; Xiong, C.; Jiang, H. Magnetic Solid-Phase Extraction Modified Quick, Easy, Cheap, Effective, Rugged and Safe Method Combined with Pre-Column Derivatization and Ultra-High Performance Liquid Chromatography-Tandem Mass Spectrometry for Determination of Estrogens and Estrogen Mimics in Pork and Chicken Samples. *J. Chromatogr. A* **2020**, *1622*, 461137. [CrossRef]
17. Cheng, Y.; Nie, J.; Liu, H.; Kuang, L.; Xu, G. Synthesis and Characterization of Magnetic Molecularly Imprinted Polymers for Effective Extraction and Determination of Kaempferol from Apple Samples. *J. Chromatogr. A* **2020**, *1630*, 461531. [CrossRef]
18. Wu, X.; Wang, X.; Lu, W.; Wang, X.; Li, J.; You, H.; Xiong, H.; Chen, L. Water-Compatible Temperature and Magnetic Dual-Responsive Molecularly Imprinted Polymers for Recognition and Extraction of Bisphenol A. *J. Chromatogr. A* **2016**, *1435*, 30–38. [CrossRef]
19. Liu, Y.; Song, W.; Zhou, D.; Han, F.; Gong, X.; Pan, P. A New Core–Shell Magnetic Mesoporous Surface Molecularly Imprinted Composite and Its Application as an MSPE Sorbent for Determination of Phthalate Esters. *RSC Adv.* **2022**, *12*, 7253–7261. [CrossRef]
20. Wu, Q.; Li, M.; Huang, Z.; Shao, Y.; Bai, L.; Zhou, L. Well-Defined Nanostructured Core–Shell Magnetic Surface Imprinted Polymers (Fe3O4@SiO2@MIPs) for Effective Extraction of Trace Tetrabromobisphenol A from Water. *J. Ind. Eng. Chem.* **2018**, *60*, 268–278. [CrossRef]
21. Bing-zhi, D.; Hua-qiang, C.; Lin, W.; Sheng-ji, X.; Nai-yun, G. The Removal of Bisphenol A by Hollow Fiber Microfiltration Membrane. *Desalination* **2010**, *250*, 693–697. [CrossRef]

22. Huang, D.; Tang, Z.; Peng, Z.; Lai, C.; Zeng, G.; Zhang, C.; Xu, P.; Cheng, M.; Wan, J.; Wang, R. Fabrication of Water-Compatible Molecularly Imprinted Polymer Based on β-Cyclodextrin Modified Magnetic Chitosan and Its Application for Selective Removal of Bisphenol A from Aqueous Solution. *J. Taiwan Inst. Chem. Eng.* **2017**, *77*, 113–121. [CrossRef]

23. Li, Y.; Li, X.; Chu, J.; Dong, C.; Qi, J.; Yuan, Y. Synthesis of Core-Shell Magnetic Molecular Imprinted Polymer by the Surface RAFT Polymerization for the Fast and Selective Removal of Endocrine Disrupting Chemicals from Aqueous Solutions. *Environ. Pollut.* **2010**, *158*, 2317–2323. [CrossRef] [PubMed]

24. Ji, Y.; Yin, J.; Xu, Z.; Zhao, C.; Huang, H.; Zhang, H.; Wang, C. Preparation of Magnetic Molecularly Imprinted Polymer for Rapid Determination of Bisphenol A in Environmental Water and Milk Samples. *Anal Bioanal. Chem.* **2009**, *395*, 1125–1133. [CrossRef] [PubMed]

25. Karrat, A.; Amine, A. Solid-Phase Extraction Combined with a Spectrophotometric Method for Determination of Bisphenol-A in Water Samples Using Magnetic Molecularly Imprinted Polymer. *Microchem. J.* **2021**, *168*, 106496. [CrossRef]

26. Xiong, H.; Guo, L.; Mao, X.; Tan, T.; Wan, H.; Wan, Y. A Magnetic Hydrophilic Molecularly Imprinted Material with Multiple Stimuli-Response Properties for Efficient Recognition of Bisphenol A in Beverages. *Food Chem.* **2020**, *331*, 127311. [CrossRef]

27. Zhang, X.; Yang, S.; Chen, W.; Li, Y.; Wei, Y.; Luo, A. Magnetic Fluorescence Molecularly Imprinted Polymer Based on FeOx/ZnS Nanocomposites for Highly Selective Sensing of Bisphenol A. *Polymers* **2019**, *11*, 1210. [CrossRef]

28. Yuan, Y.; Liu, Y.; Teng, W.; Tan, J.; Liang, Y.; Tang, Y. Preparation of Core-Shell Magnetic Molecular Imprinted Polymer with Binary Monomer for the Fast and Selective Extraction of Bisphenol A from Milk. *J. Chromatogr. A* **2016**, *1462*, 2–7. [CrossRef]

29. Zhang, Z.; Chen, X.; Rao, W.; Chen, H.; Cai, R. Synthesis and Properties of Magnetic Molecularly Imprinted Polymers Based on Multiwalled Carbon Nanotubes for Magnetic Extraction of Bisphenol A from Water. *J. Chromatogr. B* **2014**, *965*, 190–196. [CrossRef]

30. Zhu, L.-L.; Cao, Y.-H.; Cao, G.-Q. Preparation and Application of Core-Shell Magnetic Imprinted Nanoparticles for Bisphenol A. *Chin. J. Anal. Chem.* **2013**, *41*, 1724–1728. [CrossRef]

31. Rao, W.; Cai, R.; Yin, Y.; Long, F.; Zhang, Z. Magnetic Dummy Molecularly Imprinted Polymers Based on Multi-Walled Carbon Nanotubes for Rapid Selective Solid-Phase Extraction of 4-Nonylphenol in Aqueous Samples. *Talanta* **2014**, *128*, 170–176. [CrossRef] [PubMed]

32. Li, Z.; Zhang, Y.; Su, Y.; Qi, J.; Jia, Y.; Huang, C.; Dong, Q. Selective Extraction of Bisphenol A from Water by One-Monomer Molecularly Imprinted Magnetic Nanoparticles. *J. Sep. Sci.* **2018**, *41*, 2029–2036. [CrossRef]

33. Wu, X.; Li, Y.; Zhu, X.; He, C.; Wang, Q.; Liu, S. Dummy Molecularly Imprinted Magnetic Nanoparticles for Dispersive Solid-Phase Extraction and Determination of Bisphenol A in Water Samples and Orange Juice. *Talanta* **2017**, *162*, 57–64. [CrossRef] [PubMed]